ECS Journal of Solid State Science and Technology, **8** (12) P799-P804 (2019)
2162-8769/2019/8(12)/P799/6/$38.00 © The Electrochemical Society

Annealing of Proton and Alpha Particle Damage in Au-W/β-Ga_2O_3 Rectifiers

Minghan Xian,[1] Chaker Fares,[1,*] Jinho Bae,[2] Jihyun Kim,[2,] Fan Ren,[1,***] and S. J. Pearton[3,***,z]**

[1]*Department of Chemical Engineering, University of Florida, Gainesville, Florida 32611, USA*
[2]*Department of Chemical and Biological Engineering, College of Engineering, Korea University, Seoul 02841, South Korea*
[3]*Department of Material Science and Engineering, University of Florida, Gainesville, Florida 32611, USA*

Vertical geometry Ga_2O_3 rectifiers were irradiated with 18 MeV alpha particles to fluences of 1–3 × 10^{13} cm^{-2} or 10 MeV protons to fluences of 1–3 × 10^{14} cm^{-2} and then annealed to establish the thermal stability of the radiation damage. The rectifiers employed Au/W rectifying contacts to achieve the requisite thermal stability to allow for annealing studies. The carrier removal rates were ∼900 cm^{-1} for the α-particles and ∼200 for the protons. Annealing at 500°C was found to restore the carrier concentration in the α-particle irradiated devices, while 450°C annealing brought substantial recovery of the proton irradiated devices. This is a similar temperature range as established for annealing of plasma-induced damage in Ga_2O_3, suggesting a common origin of point defects, predominantly Ga vacancies and their complexes. The reverse breakdown voltages and diode on/off ratios are also significantly recovered by annealing after irradiation.
 [DOI: 10.1149/2.0231912jss]

Manuscript submitted October 31, 2019; revised manuscript received December 1, 2019. Published December 13, 2019.

There has been a tremendous amount of recent interest in the development of β-Ga_2O_3 devices[1–12] for high power electronics[13–30] and solar-blind UV photodetectors.[31–39] Initial experiments on the radiation hardness of these structures has shown that they are at least as resistant to total dose proton, neutron, electron and alpha particle effects as their GaN-based counterparts.[40–48] The ability to operate at high temperatures and powers in radiation environments is crucial to applications such as space-borne instrumentation or exploration robots in harsh environments.[49–53] The use of the radiation-hard ultra-wide bandgap semiconductor devices would mitigate some of the need for space craft shielding. For low earth orbit (LEO), the primary radiation source are the Van Allen radiation belts, which are primarily composed of high energy (≤10 MeV) protons and electrons trapped by the Earth's magnetic field.[53] Additional sources of radiation include cosmic rays and single solar events, with the primary cosmic rays, originating outside of Earth's atmosphere, being composed of protons (90%) and alpha particles (9%).[49,50,53] Single solar events occur on cycles of four inactive years of low annual fluence, followed by seven active years with fluences above 5 × 10^7 particles/cm^2 at energies >10 MeV. Previous reports on vertical geometry Ga_2O_3 rectifiers subject to 18 MeV alpha particle irradiation at fluences of 10^{12} -10^{13} cm^{-2}, simulating space radiation exposure,[54] showed the carrier removal rates were in the range 406–728 cm^{-1}, a factor of 2–3 higher than for high energy (10 MeV) protons and two orders of magnitude higher than for 1.5 MeV electron irradiation.[53] It is clearly of interest to establish the thermal stability of the damage from the most commonly encountered forms of radiation.

In this paper we report on annealing of alpha particle and proton-induced damage in vertical geometry β-Ga_2O_3 rectifiers, as determined by the restoration of initial carrier density, reverse breakdown voltage, diode on/off ratio and I-V characteristics. Near-complete recovery in both cases is obtained by annealing at 450°C for 5 min.

Experimental

The diodes were fabricated on 10 μm Si-doped (2.7 × 10^{16} cm^{-3}) epitaxial layers grown by Halide Vapor Epitaxy (HVPE) on (001) orientated 650 μm β-phase Sn-doped (n = 3.6 × 10^{18} cm^{-3}) Ga_2O_3 with edge-defined film-fed growth method (Novel Crystal Technology). A back side o contact (20 nm/80 nm Ti/Au) was formed using electron beam (E-beam) evaporation followed by 30 second rapid thermal annealing at 550°C in nitrogen ambient using an SSI SOLARIS 150 rapid thermal annealer. The sample surface was then treated in O_3 for 20 minutes to remove hydrocarbon and other contamination species. The samples were patterned again for W deposition. To allow for annealing studies, we need thermally stable rectifying contacts, so W/Au was employed, instead of the usual Ni/Au.[55] 20 nm W was deposited by dc sputtering using a 3-in. target of pure W. The dc power was 200 W and the process pressure was 5 mTorr in pure Ar ambient. Following W deposition, a 340 nm layer of Au was deposited by E-beam evaporation to reduce the sheet resistance of the contact and prevent oxidation of the tungsten. The samples were annealed at 500°C for 5 min in N_2 to remove sputtering induced damage.

For diode DC characteristics, a Tektronix 370-A curve tracer was used for forward and reverse I-V measurement. Capacitance Voltage (C-V) characteristics were recorded with an Agilent 4284A Precision LCR Meter. The on-resistance was obtained from the I-V characteristics according to

$$R_{ON}=W_D/q\mu N_D= 4(V_B)^2/\varepsilon {E_C}^3\mu$$

where V_B is the breakdown voltage, q is the electronic charge, W_D is the depletion depth, μ the electron mobility, N_D the doping in the drift region, ε the dielectric constant and E_c is the critical field for avalanche breakdown. The TLM method allows separation of sheet resistance from contact resistance since The applied current enters and leaves the sample via the outer probes. The voltmeter used has high electrical impedance, so no current will flow through the inner two probes. Only the voltage is measured between the inner probes, meaning that the probe resistances and the contact resistances do not contribute to the measurement. This simplifies the sheet resistance equation, so that only the voltage change and the applied current are required to find the value of the sheet resistance.

The 18 MeV alpha particle beam was injected into a low-vacuum chamber, where the β-Ga_2O_3-based devices were loaded, facing the beam. Fluences were fixed at 10^{12} and 10^{13} cm^{-2}. Since the alpha particles are known to be more damaging, we employed lower doses than for the protons. Proton irradiation was performed at the Korean Institute of Radiological and Medical Sciences using a Scanditronix MC 50 cyclotron. The proton energy leaving the cyclotron was 30 MeV and adjusted to reach the samples at 10 MeV by using the appropriate aluminum degraders. The irradiation was performed at two fluences, 1 × 10^{14} cm^{-2} and 3 × 10^{14} cm^{-2}, with the beam current being monitored through a Faraday cup to calculate the flux density. The average beam-current, measured by Faraday-cup, was 100 nA during the proton irradiation process. Stopping and Range of Ions in Matter (SRIM) simulations were performed to assess the electronic and nuclear stopping forces on the proton as it traversed through the devices. The

*Electrochemical Society Student Member.
**Electrochemical Society Member.
***Electrochemical Society Fellow.
[z]E-mail: spear@mse.ufl.edu

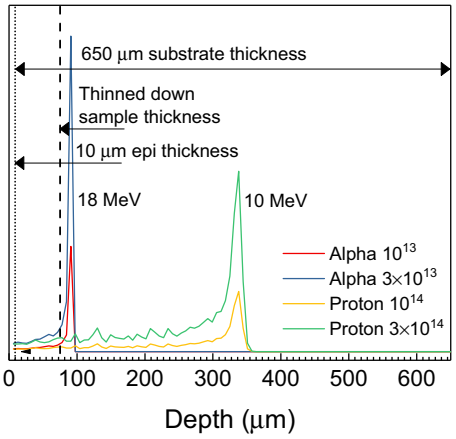

Figure 1. SRIM simulation of vacancy distribution in Ga_2O_3 subject to different fluences of 18 MeV alpha particles or 10 MeV protons. The y-axis is the relative magnitude of the vacancy density.

projected range of the alpha particle and protons beams was calculated using the Stopping and Range of Ions in Matter (SRIM) program and is 85 and 340 µm, respectively, as shown in Figure 1. This means the alpha particles and protons completely traverse the drift region of the rectifiers and come to rest in the substrate. In other words, the damage is mainly beyond the drift region.

To gain some perspective of how much damage remained in the drift region of the rectifiers, we thinned down some of the samples by polishing removal of most of the substrate until just 75 µm thickness remained and then metallized the back side. Schematics of the full thickness and thinned rectifiers is shown in Figure 2. Table I summarizes the effect of both types of radiation exposure on the Schottky barrier height, diode ideality factor and on-state resistance for the as-irradiated and annealed conditions. The differences in these parameters are generally smaller than for the I-V, C-V and on/off ratios of the rectifiers, so we focus on that data in the subsequent sections.

Results and Discussion

Alpha -particle irradiated rectifiers.—Figure 3 shows the forward I-V characteristics for the rectifiers before and after the 10^{13} cm^{-2} (top)

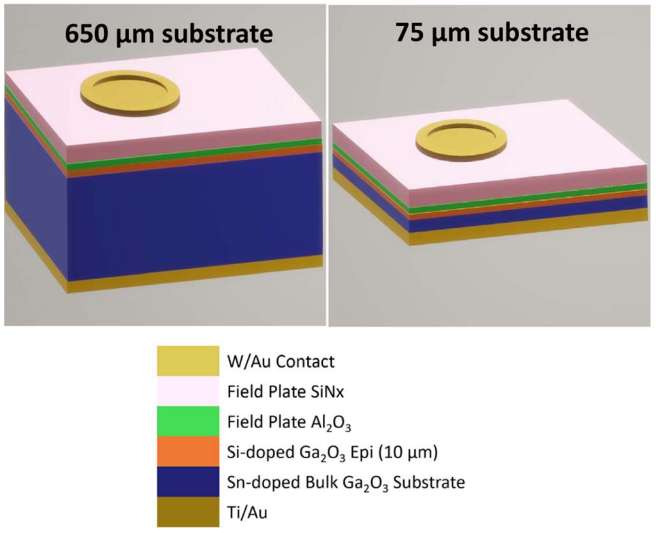

Figure 2. Schematic of conventional (left) and thinned-down (right) rectifier structures.

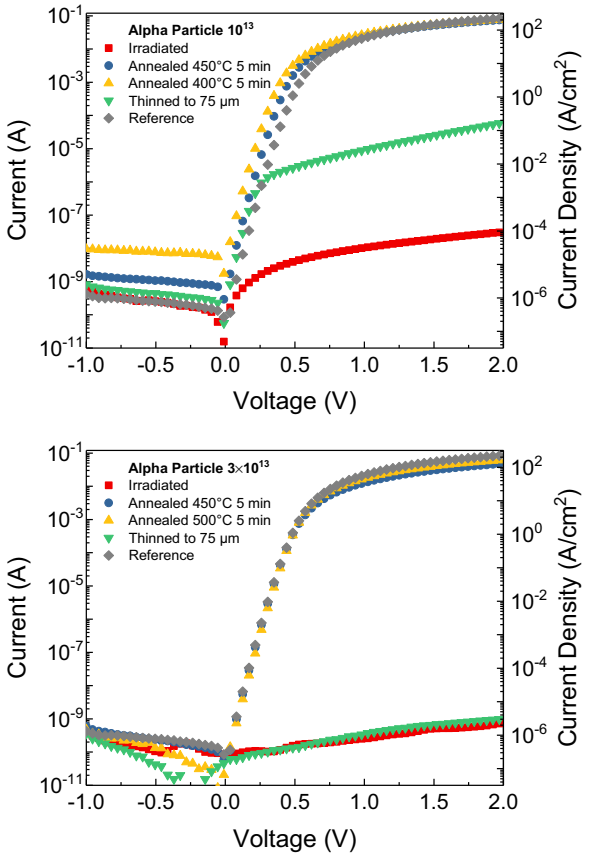

Figure 3. Rectifier forward I-V characteristics before and after alpha particle irradiation at a fluence of 10^{13} cm^{-2} (top) or 3×10^{13} cm^{-2} (bottom) and after subsequent annealing at 400–500°C.

and 3×10^{13} cm^{-2} (bottom) fluences and after subsequent annealing. The main effect of the irradiation is to reduce the forward current. Since the total forward current is proportional to $e\mu_n nE$, where e is the electronic charge, μ_n is the electron mobility, n is the carrier concentration and E is the electric field strength at a given bias voltage, then the reduction in forward current is due to a reduction in both mobility and carrier concentration,[2,6] the latter through formation of deep trapping states that remove electrons from the conduction band. This is consistent with previous work in other wide bandgap semiconductors, where both mobility and carrier density are observed to diminish as a result of the introduction of radiation damage.[48–53] The thinned diodes suffer less current reduction for the low dose, but the higher dose suppresses current to a similar level as in the regular thickness devices since the damage is basically saturated. It is noteworthy that annealing at 500°C for 5 min is basically sufficient to restore the forward current. Previous reports have shown that plasma-induced damage in Ga_2O_3 also anneals in this temperature range,[44] suggesting a common origin of point defects. In particular, Ga_v acceptors are among the dominant defects present in Ga_2O_3, even in the as-grown state.[56–58] The electrical compensation in n-type Ga_2O_3 is found to be dominated by the presence of Ga vacancies, with V_{Ga}.[59–61]

Figure 4 shows the reverse current characteristics for the higher dose samples. Assuming a one-sided abrupt diode, the corresponding breakdown voltage, V_B is proportional to $E_B{}^2.\varepsilon/2en$, where E is the electric field at breakdown, and ε is the permittivity of the semiconductor.[6] Thus, the reduction in carrier density will cause an increase in breakdown voltage. Once again, annealing at 500°C is sufficient to restore the initial breakdown characteristics.

The recovery in carrier concentration as a function of annealing was obtained from C-V measurements, with the results shown in Figure 5 in the form of C^{-2}-V plots. The drift layer became fully depleted

Table I. Summary of barrier heights, ideality factors and on-state resistances.

Irradiation Dose	Sample	Schottky Barrier Height (eV)	Ideality Factor (-)	On Resistance (mΩ∗cm^2)
Reference	Reference	0.77	1.15	4.9
Alpha 10^{13}	Irradiated	0.68	1.23	17.8
	450°C 5 min anneal	0.7	1.2	6.3
	400°C 5 min anneal	0.65	1.29	6.3
	Thinned down	0.74	1.12	745
Alpha 3×10^{13}	Irradiated	0.66	1.28	19.0
	450°C 5 min anneal	0.79	1.12	8.6
	500°C 5 min anneal	0.79	1.12	6.9
Proton 10^{14}	Irradiated	0.74	1.12	16.9
	450°C 5 min anneal	0.76	1.09	6.4
Proton 3×10^{14}	Irradiated	0.74	1.13	13.1
	450°C 5 min anneal	0.82	1.09	7

for both the alpha fluences, but recovered with annealing. Consistent with the I-V data, the carrier concentration is seen to be restored to essentially its initial level after 500°C annealing. The starting carrier concentration in the drift region of the as-fabricated diodes was 2.69 $\times$ 10^{16} cm^{-3} and in the higher dose samples, this recovered to 1.33 $\times$ 10^{16} cm^{-3} for annealing at 450°C and 2.67 $\times$ 10^{16}cm^{-3} for 500°C annealing.

The diode on/off ratio is another figure-of-merit. Figure 6 shows this ratio when switching from 2V forward to the reverse bias shown on the x-axis for the 10^{13} (top) and 3×10^{13} cm^{-2} (bottom) fluences ad the recovery with annealing. The on/off ratio is particularly susceptible to change with the introduction of radiation damage, decreasing by 6–8 orders of magnitude depending on the alpha particle fluence. However,

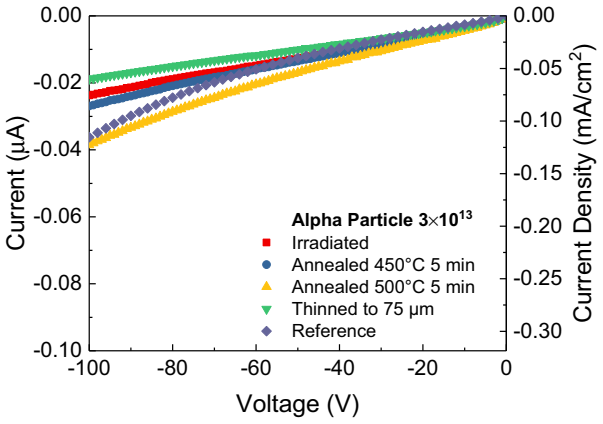

Figure 4. Reverse I-V characteristics before and after alpha particle irradiation at a fluence of 3×10^{13} cm^{-2} and after subsequent annealing at 450–500°C.

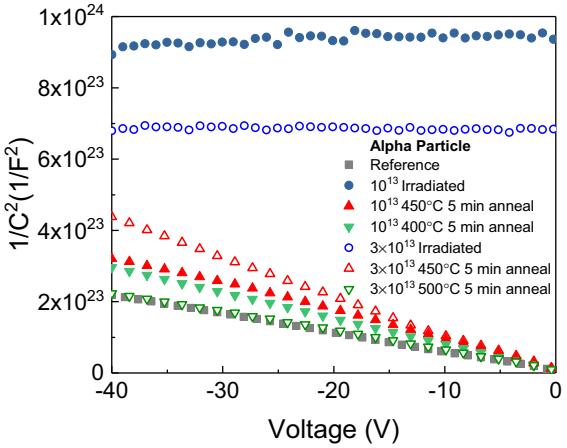

Figure 5. C^{-2}-V plots for rectifiers before and after alpha particle irradiation and subsequent annealing.

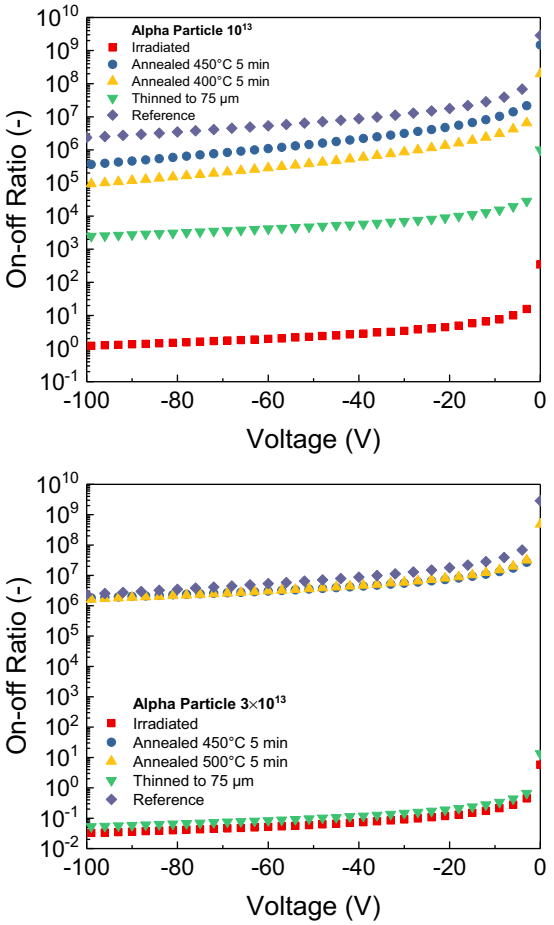

Figure 6. On/off ratio when switching from 2 V forward bias to the reverse biases shown on the x-axes, for alpha particle fluences of 10^{13} (top) or 3×10^{13} cm^{-2} (bottom).

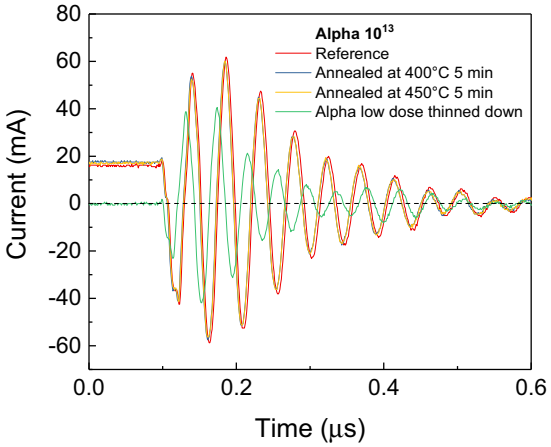

Figure 7. Time response of alpha irradiated (10^{13} cm^{-2} fluence) rectifiers when switching from 18 mA forward current to −6 V, showing a reverse recovery time τrr, of ∼20 nsec.

the annealing treatments are effective in restoring the original values. Figure 7 shows the time response of the rectifiers[62,63] when switched from ∼18 mA forward current to a reverse bias of -6V. There was little change as a result of irradiation with alpha particles or subsequent annealing and the only measurable differences are observed with the thinned down sample because of its lower capacitance.

Proton irradiated rectifiers.—The effects of proton irradiation were much less pronounced than for the alpha particle irradiation. Figure 8 shows the forward I-V characteristics for the 10^{14} (top) and 3×10^{14} (center) fluences, as well as the reverse characteristics (bottom). There are only small reductions in forward current, which was restored by annealing at 450°C. Similar trends are seen in the reverse current.

Figure 9 shows the C^{-2}-V plots for the proton irradiated samples and their change with annealing. The carrier concentration recovered to 2.1 ±0.5 × 10^{16} cm^{-3} for annealing at 450°C, which within the error of the initial value prior to irradiation.

The carrier removal rate N_R was calculated from the change in sheet carrier density as a result of irradiation with fluence Φ, according to[49,50]

$$N_R = \frac{n_{s0} - n_s}{\Phi}$$

The results are summarized in Figure 10 for both the protons and alpha particle irradiations performed in this work, as well as a collection of the previously reported values.[53] The trend is that alpha particles are the most damaging form of radiation, as measured by carrier removal rate, followed by protons and then neutrons, electrons and gamma rays. We obtained removal rates of 897 cm^{-1} for 18 MeV alpha particle and 203 for 10 MeV protons, consistent with previous reports. For annealing, we obtained typical recoveries of ∼50% for annealing of both proton and alpha particle-induced damage at 450°C and 100% for annealing at 500°C.

Figure 11 shows the on/off ratios when switching from 1 V forward bias to the reverse biases shown on the x-axes, for proton fluences of 10^{14} or 3×10^{13} cm^{-2}. The degradation in this ratio is much smaller than for alpha particles, with less than an order of magnitude decrease over most of the reverse bias range investigated. Annealing at 450°C does not fully restore the pre-irradiated values but they are back to >90% of these values.

Finally, we looked at the time-dependent current recovery switching characteristics when switching from forward current to reverse bias.[62,63] Figure 12 shows the rectifier switching response when switched from 18 mA forward current to a reverse voltage of −6 V. The recovery time was ∼20 ns with a dI/dt of 6 A/µs for both the

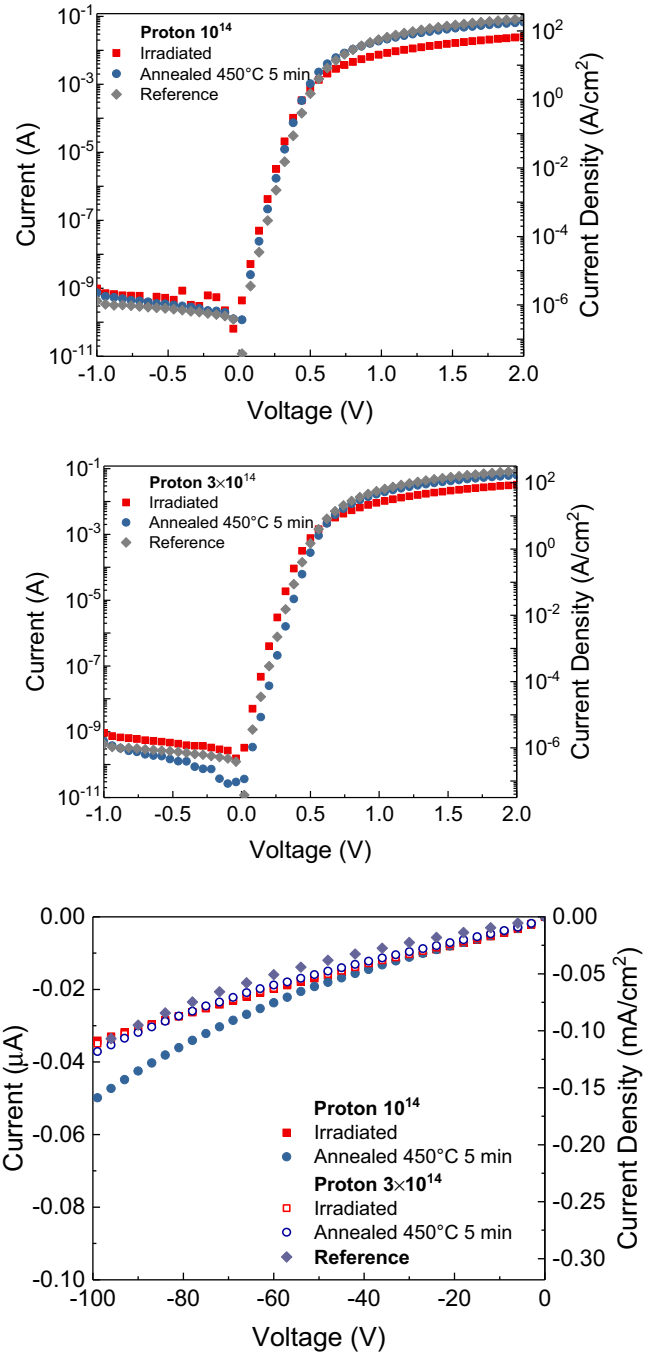

Figure 8. Rectifier forward I-V characteristics before and after proton irradiation at a fluence of 10^{14} cm^{-2} (top) or 3×10^{14} cm^{-2} (center) and after subsequent annealing at 450°C, as well as the reverse I-Vs under similar conditions (bottom).

reference and irradiated/annealed rectifiers. The high proton dose did reduce the forward current under these conditions.

Conclusions

The thermal stability of radiation damage in Ga_2O_3 vertical rectifiers was established for alpha and proton-irradiation. The I-V, C-V and on/off ratios are all significantly degraded by moderate fluences of these forms of radiation, but can be essentially recovered by annealing at 450°C for 5 mins. Other parameters such as Schottky barrier height, ideality factor and reverse recovery char-

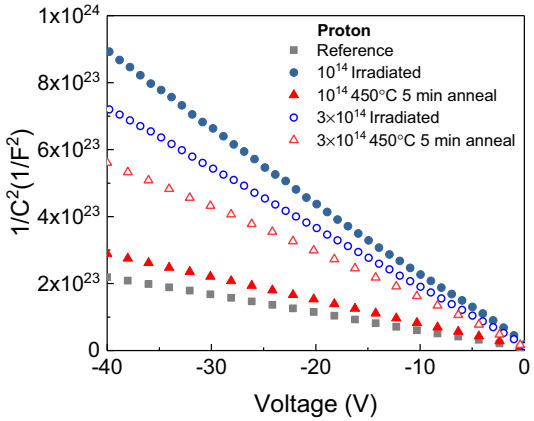

Figure 9. C^{-2}-V plots for rectifiers before and after proton irradiation and subsequent annealing.

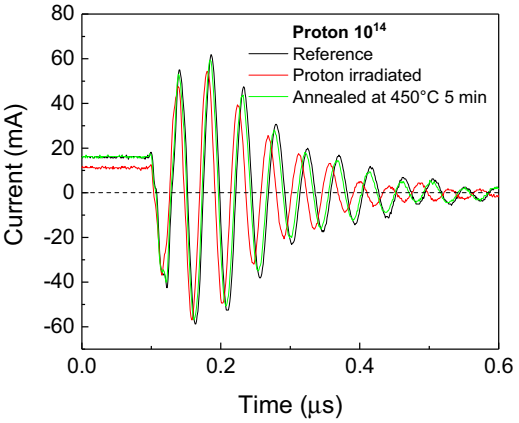

Figure 12. Time response of proton irradiated rectifiers when switching from 18 mA forward current to −6 V, showing a reverse recovery time τrr, of ∼20 nsec.

acteristics are less affected by radiation damage. The commonality of annealing stages between these ionizing forms of radiation and plasma -induced damage in Ga_2O_3 suggest a common origin of point defects. In the vertical geometry devices studied here, the damage created in the drift region is most important in determining the relative degradation of device performance, as evidenced by our experiments where were removed the end-of-range damage in the substrate.

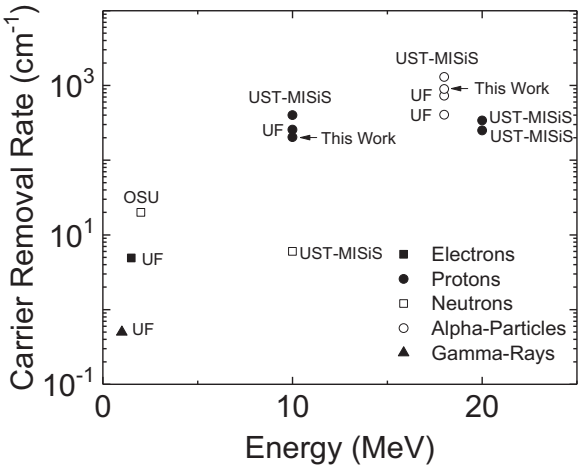

Figure 10. Collection of reported carrier removal rate for vertical geometry Ga_2O_3 rectifiers irradiated with protons, electrons, neutrons gamma rays or alpha particles, including the results obtained in this work.

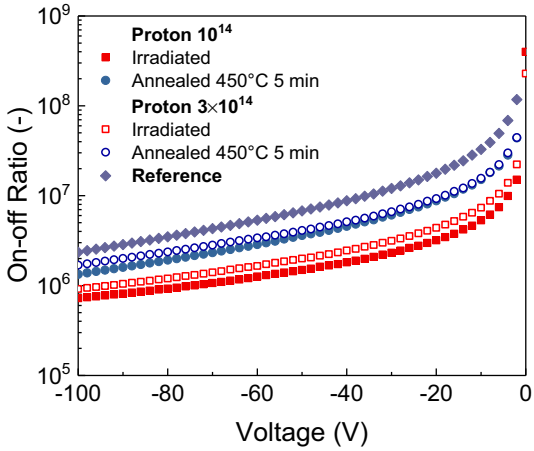

Figure 11. On/off ratio when switching from 2V forward bias to the reverse biases shown on the x-axes, for proton fluences of 10^{14} or 3×10^{13} cm^{-2}.

Acknowledgments

The work at UF was partially sponsored by the Department of the Defense, Defense Threat Reduction Agency, No. HDTRA1-17-1-011, monitored by Jacob Calkins and also by NSF DMR 1856662 (Tania Paskova).The research at Korea University was supported by the National Research Foundation of Korea (2018R1D1A1A09083917) and the Korea Institute of Energy Technology Evaluation and Planning (KETEP) (20172010104830).

ORCID

Chaker Fares https://orcid.org/0000-0001-9596-2381
Jihyun Kim https://orcid.org/0000-0002-5634-8394
S. J. Pearton https://orcid.org/0000-0001-6498-1256

References

1. Zbigniew Galazka, *Semicond. Sci. Technol.*, **33**, 113001 (2018).
2. S. J. Pearton, Jiancheng Yang, Patrick H. Cary IV, F. Ren, Jihyun Kim, Marko J. Tadjer, and Michael A. Mastro, *App. Phys. Rev.*, **5**, 011301 (2018).
3. S. I. Stepanov, V. I. Nikolaev, V. E. Bougrov, and A. E. Romanov, *Rev. Adv. Mater. Sci.*, **44**, 63 (2016).
4. M. A. Mastro, A. Kuramata, Jacob Calkins, Jihyun Kim, Fan Ren, and S. J. Pearton, *ECS J. Solid State Sci. Technol.*, **6**, P356 (2017).
5. H. Von Wenckstern, *Adv. Electron. Mater.*, **3**, 1600350 (2017).
6. J. Y. Tsao, S. Chowdhury, M. A. Hollis, D. Jena, N. M. Johnson, K. A. Jones, R. J. Kaplar, S. Rajan, C. G. Van de Walle, E. Bellotti, C. L. Chua, R. Collazo, M. E. Coltrin, J. A. Cooper, K. R. Evans, S. Graham, T. A. Grotjohn, E. R. Heller, M. Higashiwaki, M. S. Islam, P. W. Juodawlkis, M. A. Khan, A. D. Koehler, J. H. Leach, U. K. Mishra, R. J. Nemanich, R. C. N. Pilawa-Podgurski, J. B. Shealy, Z. Sitar, M. J. Tadjer, A. F. Witulski, M. Wraback, and J. A. Simmons, *Adv. Electronic Mat.*, **4**, 1600501(2018).
7. Masataka Higashiwaki and Gregg H, Jessen, *Appl. Phys. Lett.*, **112**, 060401 (2018).
8. S. J. Pearton, F. Ren, M. Tadjer, and J. Kim, *J. Appl. Phys.*, **124**, 220901 (2018).
9. M. A. Mastro, J. K. Hite, C. R. Eddy, M. J. Tadjer, S. J. Pearton, F. Ren, and J. Kim, *Int. J. High Speed Electronics and Sys.*, **28**, 1940007 (2019).
10. B. Bayraktaroglu, Assessment of Ga_2O_3 Technology, Air Force Research Lab, Devices for Sensing Branch, Aerospace Components & Subsystems Division, Report AFRL-RY-WP-TR-2017-0167 (2017).
11. M. H. Wong and M. Higashiwaki, *Int. J. High Speed Electron Syst.*, **28**, 1940002 (2019).
12. Md Nazmul Hasan, Edward Swinnich, and Jung-Hun Seo, *Int. J. High Speed Electron Syst.*, **28**, 1940004 (2019).
13. J. Yang, F. Ren, M. Tadjer, S. J. Pearton, and A. Kuramata, *AIP Advances*, **8**, 55026 (2018).
14. J. Yang, S. Ahn, F. Ren, S. J. Pearton, S. Jang, and A. Kuramata, *IEEE Electron Dev. Lett.*, **38**, 906 (2017).

15. J. Yang, F. Ren, M. Tadjer, S. J. Pearton, and A. Kuramata, *ECS J. Solid State Sci. Technol.*, **7**, Q92 (2018).
16. Yangyang Gao, Ang Li, Qian Feng, Zhuangzhuang Hu, Zhaoqing Feng, Ke Zhang, and Xiaoli Lu, *Nanoscale Res. Lett.*, **14**, 8 (2019).
17. J. C. Yang, Minghan Xian, Patrick Carey, Chaker Fares, J. Partain, Fan Ren, Marko Tadjer, E. Anber, D. Foley, A. Lang, J. Hart, J. Nathaniel, M. L Taheri, S. J. Pearton, and Akito Kuramata, *Appl. Phys. Lett.*, **114**, 232106 (2019).
18. Z. Hu, K. Nomoto, W. Li, N. Tanen, N. Sasaki, A. Kuramata, T. Nakamura, D. Jena, and H. G. Xing, *IEEE Electron Dev. Lett.*, **39**, 869 (2018).
19. Ang Li, Qian Feng, Jincheng Zhang, Zhuang Hu, Zhaoqing Feng, Ke Zhang, Chunfu Zhang, Hong Zhou, and Yue Hao, *Superlattices and Microstructures*, **119**, 212 (2018).
20. K. Sasaki, Q. T. Thieu, D. Wakimoto, Y. Koishikawa, A. Kuramata, and S. Yamakoshi, *Appl. Phys. Express*, **10**, 124201 (2017).
21. W. Li, Z. Hu, K. Nomoto, R. Jinno, Z. Zhang, T. Q. Tu, K. Sasaki, A. Kuramata, D. Jena, and H. G. Xing, 2.44 kV Ga_2O_3 vertical trench Schottky barrier diodes with very low reverse leakage current, 2018 IEEE Int. Electron Devices Meeting (IEDM), pp. 8.5.1 (2018)
22. Q. He, W. Mu, B. Fu, Z. Jia, S. Long, Z. Yu, Z. Yao, W. Wang, H. Don, and Y. Qin, *IEEE Electron Dev. Lett.*, **39**, 556 (2018).
23. G. Jian G, Q. He, W. Mu, B. Fu, H. Dong, Y. Qin, Y. Zhang, H. Xue, S. Lon, and Z. Jia, *AIP Adv*, **8**, 015316 (2018).
24. Zongyang Hu, Kazuki Nomoto, Wenshen Li, Nicholas Tanen, Kohei Sasaki, Akito Kuramata, Tohru Nakamura, Debdeep Jena, and Huili Grace Xing, *IEEE Electron Dev. Lett.*, **39**, 869 (2018).
25. Minghan Xian, Randy Elhassani, Chaker Fares, Fan Ren, Marko Tadjer, and S. J. Pearton, *J. Vac. Sci. Technology B*, **37**, 061205 (2019);
26. J. Yang, S. Ahn, F. Ren, S. J. Pearton, S. Jang, J. Kim, and A. Kuramata, *Appl. Phys. Lett.*, **110**, 192101 (2017).
27. J. Yang, S. Ahn, F. Ren, S. J. Pearton, S. Jang, and A. Kuramata, *IEEE Electron. Dev. Lett.*, **38**, 906 (2017).
28. K. Konishi, K. Goto, H. Murakami, Y. Kumagai, A. Kuramata, S. Yamakoshi, and M. Higashiwaki, *Appl. Phys. Lett.*, **110**, 103506 (2017).
29. S. Oh, J. Kim, F. Ren, and S. J. Pearton, *J. Mater. Chem. C*, **4** 9245 (2016).
30. S. Oh, M. Mastro, M. J. Tadjer, and J. Kim, *ECS J. Solid State Sci. Technol.*, **6** Q79 (2017).
31. T.-C. Wei, D.-S. Tsai, P. Ravadgar, Jr-Jian Ke, M.-L. Tsai, D.-H. Lien, C.-Y. Huang, R.-H. Horng, and Jr-Hau He, *IEEE J. Sel. Top. Quantum Electron.*, **20** 112 (2014).
32. T. Oshima, T. Okuno, N. Arai, N. Suzuki, S. Ohira, and S. Fujita, *Appl. Phys. Express* **1**, 011202 (2008).
33. S. Oh, C. K. Kim, and J. Kim, *ACS Photonics*, **5**, 1123 (2018).
34. S. Ahn, F. Ren, S. Oh, Y. Jung, J. Kim, M. A. Mastro, J. K. Hite, C. R. Eddy, and S. J. Pearton, *J. Vac. Sci. Technol. B*, **34**, 041207 (2016).
35. M. Chen, J. Ma, P. Li, H. Xu, and Y. Liu, *Opt. Express*, **27**, 8717 (2019).
36. T. He, X. Zhang, X. Ding, C. Sun, Y. Zhao, Q. Yu, J. Ning, R. Wang, G. Yu, S. Lu, K. Zhang, X. Zhang, and B. Zhang, *Adv. Opt. Mater.*, 1801563 (2019).
37. B. Zhao, F. Wang, H. Chen, L. Zheng, L. Su, D. Zhao, and X. Fang, *Adv. Funct. Mater.*, **27** 1700264 (2017).
38. Y. Chen, Y. Lu, C. Lin, Y. Tian, C. Gao, L. Dong, and C. Shan, *J. Mater. Chem. C*, **6**, 5727 (2018).
39. S. Ahn, Y.-H. Lin, F. Ren, S. Oh, Y. Jung, G. Yang, J. Kim, M. A. Mastro, J. K. Hite, C. R. Eddy, and S. J. Pearton, *J. Vac. Sci. Technol. B*, **34**, 041213 (2016).
40. D. Szalkai, Z. Galazka, K. Irmscher, P. Tüttő, A. Klix, and D. Gehre, *IEEE T Nucl. Sci.*, **64**, 1574 (2017).
41. J. Yang, F. Ren, S. J. Pearton, G. Yang, J. Kim, and A. Kuramata, *J. Vac. Sci. Technol. B*, **35**, 031208 (2017).
42. E. Farzana, M. F. Chaiken, T. E. Blue, A. R. Arehart, and S. A. Ringel, *APL Materials*, **7**, 022502 (2019).
43. G. Yang, S. Jang, F. Ren, S. J. Pearton, and J. Kim, *ACS Appl. Mater. Interfaces*, **9**, 40471 (2017).
44. J. Yang, F. Ren, R. Khanna, K. Bevlin, D. Geerpuram, Li-Chun Tung, Jingyu Liu, Hongxing Jiang, J. Lee, E. Flitsiyan, L. Chernyak, S. J. Pearton, and A. Kuramata, J. Vac, *Sci. Technol. B*, **35**, 051201 (2017).
45. J. Yang, Zhiting Chen, F. Ren, S. J. Pearton, Gwangseok Yang, Jihyun Kim, J. Lee, E. Flitsiyan, Leonid Chernyak, and A. Kuramata, *J. Vac. Sci. Technol., B*, **36**, 011206 (2018).
46. A. Y. Polyakov, N. B. Smirnov, I. V. Shchemerov, E. B. Yakimov, Jiancheng Yang, F. Ren, Gwangseok Yang, J. Kim, A. Kuramata, and S. J. Pearton, *Appl. Phys. Lett.*, **112**, 032107 (2018).
47. J. D. Lee, Elena Flitsiyan, Leonid Chernyak, J. Yang, Fan Ren, S. J. Pearton, B. Meyler, and Y. J. Salzman, *Appl. Phys. Lett.*, **112**, 082104 (2018).
48. P. Hazdra and S. Popelka, *Phys. Status Solidi (a)*, **214**, 1600447 (2017).
49. S. J. Pearton, F. Ren, E. Patrick, M. E. Law, and A. Y. Polyakov, *ECS J. Solid State Science and Technol.*, **5**, Q35 (2016).
50. B. D. Weaver, P. A. Martin, J. B. Boos, and C. D. Cress, *IEEE Trans. Nucl. Sci.*, **59**, 3077 (2012).
51. D. Keum and H. Kim, *Semicond. Technol. Sci.*, **19**, 214 (2019).
52. E. Patrick, M. Law, L. Liu, C. Cuervo, Y. Xi, F. Ren, and S. J. Pearton, *IEEE Trans. Nucl. Sci.*, **60**, 4103 (2013).
53. Jihyun Kim, S. J. Pearton, Chaker Fares, Jiancheng Yang, Fan Ren, Suhyun Kim, and A. Y. Polyakov, *J. Mat. Chem., C*, **7**, 10 (2019).
54. J. Yang, Chaker Fares, Yu Guan, F. Ren, S. J. Pearton, Jinho Bae, Jihyun Kim, and Akito Kuramata, *J. Vac. Sci. Technol. B.*, **36**, 031205 (2018).
55. Minghan Xian, Chaker Fares, Fan Ren, P. Brent, Gila, Yen-Ting Chen, Yu-Te Liao, Marko Tadjer, and S. J. Pearton, *J. Vac. Sci Technol. B*, **37**, 061201 (2019).
56. E. Korhonen, F. Tuomisto, D. Gogova, G. Wagner, M. Baldini, Z. Galazka, R. Schewski, and M. Albrecht, *Appl. Phys. Lett.*, **106**, 242103 (2015).
57. B. E. Kananen, L. E. Halliburton, K. T. Stevens, G. K. Foundos, K. B. Chang, and N. C. Giles, *Appl. Phys. Lett.*, **110**, 202104 (2017).
58. B. E. Kananen, N. C. Giles, L. E. Halliburton, G. K. Foundos, K. B. Chang, and K. T. Stevens, *Journal of Applied Physics*, **122**, 215703 (2017).
59. A. Kyrtsos, M. Matsubara, and E. Bellotti, *Phys. Rev. B*, **95**, 245202 (2017).
60. A. Y. Polyakov, N. B. Smirnov, I. V. Shchemerov, D. Gogova, S. A. Tarelkin, and S. J. Pearton, *J. Appl. Phys.*, **123**, 115702 (2018).
61. J. B. Varley, J. R. Weber, A. Janotti, and C. G. Van de Walle, *Appl. Phys. Lett.*, **97**, 142106 (2010).
62. Yen-Ting Chen, J. C. Yang, Fan Ren, Chin-Wei Chang, Jenshan Lin, S. J. Pearton, Marko J. Tadjer, Akito Kuramata, and Yu-Te Liao, *ECS J. Solid State Sci. Technol.*, **8**, Q3229 (2019).
63. J. Yang, F. Ren, Y. Chen, Y. Liao, C. Chang, J. Lin, M. Tadjer, S. J. Pearton, and A. Kuramata, *IEEE J. Electron Dev. Soc.*, **7**, 57 (2019).